Renewable Energy 139 (2019) 1029–1039

Contents lists available at ScienceDirect

Renewable Energy

journal homepage: www.elsevier.com/locate/renene

Flow induced noise characterization of pump turbine in continuous and intermittent load rejection processes

Xiuli Mao [a, *], Giorgio Pavesi [b], Diyi Chen [a], Hengshan Xu [a], Gaojun Mao [c]

[a] Institute of Water Resources and Hydropower Research, Northwest A & F University, 712100 Yangling, China
[b] Department of Industrial Engineering, University of Padova, Padova 35131, Italy
[c] State Key Laboratory of Advanced Processing and Recycling of Non-ferrous Metals, Lanzhou University of Technology, Lanzhou 730050, China

ARTICLE INFO

Article history:
Received 5 October 2018
Received in revised form
25 December 2018
Accepted 21 February 2019
Available online 26 February 2019

Keywords:
Hydroelectric energy
Pump turbine
Load rejection
Pressure fluctuations
Flow induced noise

ABSTRACT

In order to study pump turbine stability in view of flow induced noise, this paper focuses on two-part operation of one high head reversible turbine: transient load rejection process and intermittent vane closing conditions. Both above simulations are solved by DES turbulent model, additionally, the flow field results are regarded as sound source and analyzed comparatively by LMS software. Except for flow field interpretation, some developing rules of flow induced noise during the period of pump turbine load rejection are found. The result indicates that flow induced noise radiation is consistent with internal fluid characteristics, and the developing trends are similar which acquired from these two part calculations, whereas the values are distinct. This work provides a reference for the study of pump turbine operating stability from the acoustic aspect, and for pump turbine design work as well.

1. Introduction

Operating stability of renewable energy is a key issue at present, which should be payed more attention from the standpoint of ongoing electricity market reforms [1]. For the purpose of balancing load variations and improving grid stability that caused by renewable energies, the number of pumped storage plants maintains an increasing trend in recent years [2]. Pumped storage units are moving toward the high head, large capacity and high speed to obtain better economic efficiency [3]. Consequently, the pumped storage plant safe operation becomes extremely important and urgent problem that needs to be solved, which root is complicated flow field characteristics of machinery [4].

The flow field analysis is the hot topic in the study of hydraulic machinery performance. For example, the work of Olimstad shows the output of system not only depends on the input variables, but also the flow state of the previous operating condition [5]. Pavesi et al. proposed wall siding mesh technique to analyse internal flow field characteristics of one reversible pump turbine in the load rejection process [6]. Holler obtained a remarkably good agreement between experimental and numerical results [7]. Walseth measured dynamic characteristics of a reversible pump turbine model, the results illustrate that pump turbine experienced damped oscillations in pressure, speed and flow rate around runaway [8]. Guo used LES turbulent model based on Vreman subgrid-scale model to capture flow characteristics in one Francis turbine near wall zones in guide vane domain [9]. Liu investigated generation and development of backflow in axial and radial directions of pump turbine with two guide vane openings [10]. Rezghi analyzed the inertia moment on the maximum torque at runaway condition of two parallel pump turbines [11]. Chen presented a novel nonlinear mathematical model for governing system of one turbine in the process of load rejection [12]et al. However, few published papers clarify rotor-rotor interaction influence on flow field, and sound field characteristic of pump turbine which operating in transient processes, even flow induced noise is related to flow field structure, cavitation, water hammer [13] et al.

The main part of reducing pump turbine noise is flow induced noise reduction, for the reason of mechanical noise can be controlled by improving machinery precision and installation accuracy [14]. Chu identified primary noise sources in a centrifugal pump, the flow induced noise propagates in piping system and generates structure-borne noise through vibro-acoustic coupling [15]. Yamade used Lighthills acoustic analogy to compute sound that caused by flows with low mach number [16]. A series of tests

* Corresponding author.
E-mail address: maoxl@nwafu.edu.cn (X. Mao).

https://doi.org/10.1016/j.renene.2019.02.116
0960-1481/

were carried out by Jorge to validate an acoustic model which presented in his paper, this model aims at estimating the low frequency pressure fluctuations in one centrifugal pump [17]. Liu adopted CFD methods to investigate the influence from four different surface dipole sources in a centrifugal pump on the acoustic calculating accuracy [18]. In Yang's paper, noise simulation method has been proved as a good way to predict and optimize the hydroacoustic behavior of centrifugal pump [19]. Yet still only fixed conditions are performed in the previous works for analyzing flow induced noise, and few works are related to sound source generated from transient flow fields of pump turbine.

In light of these considerations, the main concern of this paper is analyzing flow induced noise of pump turbine during the period of load rejection. Similar works are performed under fixed vane openings as well. LMS software is adopted to study sound field, due to experimental study on this issue is unacceptable for industrial applications with unsustainable cost. CFX is utilized in flow field calculation for the following two reasons: experimental study is not available to full visualization; after pump turbine running for a long period, guide vanes can not be attached in the end of closure on account of abrasion.

2. Description of numerical model and setup

2.1. Numerical model and mesh

Fig. 1 shows the RPT(Reversible pump turbine) model with one inlet pipe, 20 fixed blades in return channels, 20 adjustable vanes in guide vane domain, one runner with 7 backward 3D blades and one draft tube. Table 1 presents the main parameters of this considered model.

The entire computational domain is divided with structured mesh by ICEM software, all blades in different domains adopt O-blocks to mesh. For ensuring the capacity of numerical simulation to capture details of pressure fluctuations, different mesh sizes are applied in mesh sensitivity test(Fig. 2). The sensitivity analysis obtains a mesh independent solution at Fig. 2 A, the intensity and extent of the local pressure pulsations appear to be correctly

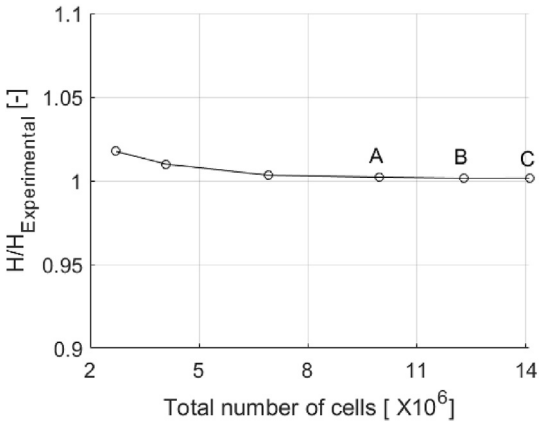

Fig. 2. Mesh sensitivity test based on the head acquired from experiments and simulations:A10 $\times$ 10^6 B12.35 $\times$ 10^6 C14 $\times$ 10^6.

evaluated only with mesh elements more than 3×10^5 of each passage (Fig. 2 B). In order to guarantee the capacity of numerical solution for capturing local pressure pulsations in the whole domain well, the adopted number of elements is further increased around 14×10^6 elements totally(Fig. 2 C).

Fig. 3 shows pump turbine meshes in some regions. The mesh size of return channels is around 5.11×10^6, guide vane domain with about 3.55×10^6 cells and the runner mesh cells is 3.7×10^6 approximately, a structured mesh is built on draft tube with about 3.25×10^5 elements. Furthermore, the labyrinth seal is also modelled by several H-blocks due to the influence of leakage flow rate at partial loads needs to be considered. More details about mesh part context is similar to Ref. [6].

2.2. Model validation and numerical setup

Steady simulation at BEP condition with a constant rotating speed is performed to validate this model, the head values are

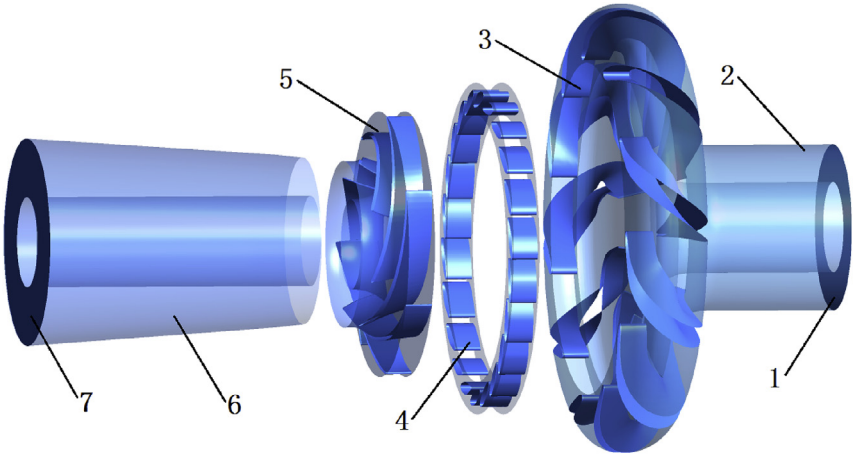

Fig. 1. Three dimensional RPT model:1 Inlet,2 Inlet pipe,3 Return channels,4 Guide vane,5 Runner,6 Draft tube,7 Outlet.

Table 1
Main parameters of the RPT model.

Runner data				Guide vanes data				Return channels data			
D_{RI}	B_{RI}	n_R	α_{RI}	D_{GVO}	B_{GVO}	n_{GV}	α_{GV}	D_{RTO}	B_{RTO}	n_{RT}	α_{RT}
400	40	7	26.5	410	40	22	23.44	516	40	11	30

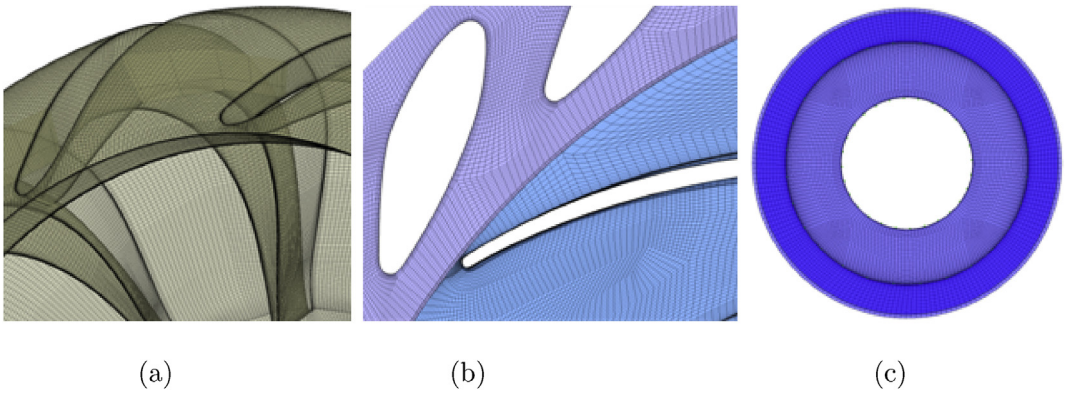

Fig. 3. Structured mesh in some regions of the RPT in the flow field: (a) Return channels, (b) Guide vane and runner, (c) Draft tube.

compared between numerical and experimental results according to ISO standards. Calibrations of instruments are performed in site, the global measurements of flow, head and efficiency are conducted based on IEC recommendations: 0.1% precision for efficiency near to BEP and 0.3% for the off design conditions.

A quasi-steady simulation has been achieved after running more than 20 revolutions, the numerical data are obtained by averaging the results of 10 impeller revolutions. The differences between experimental data and simulating results are limited not only at BEP, but also at part load conditions. The averaged numerical result agrees quite well with experimental result in terms of head, with an error lower than 0.2% near to BEP and smaller than about 3.3% at part loads (Fig. 4). Compared with simulations of incompressible flow, all simulations that considered water weak compressibility obtained a little better agreement. Therefore, weakly compressible water is used in the simulation of pump turbine load rejection.

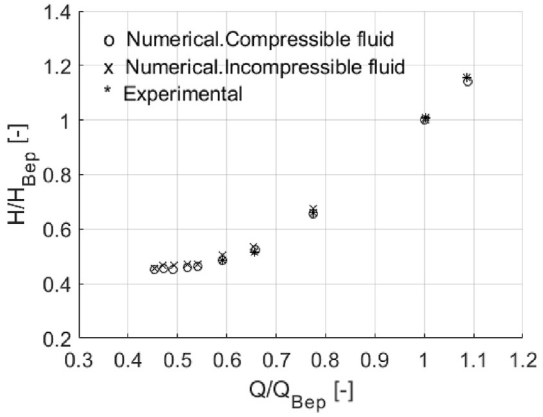

Fig. 4. Comparison of the RPT head values in different conditions between numerical and experimental data.

In this research, for realizing guide vane closure(Fig. 5(b), Motion 1), all guide vanes are set to rotate around their respective axes according to closing law(Fig. 5(a)). In the meantime, mesh nodes move along guide vane profile in the opposite direction of vane closure proportionally(Fig. 5(b), Motion 2). Above two motions belong to the content of wall sliding mesh technique, which is a weighted diagnostic between determinant, orthogonality and warp.

Based on the previous work [6], DES turbulent model is utilized in the simulation of load rejection period due to it is able to capture fluid details in transient process, which has been applied in many industrial cases as well[[20,21]]. Guilmineau applied several versions of the DES models based on the $k-\omega$ SST turbulence mode, and a better solution of the main flow features is given [22]. Xu used the Wray-Agarwal turbulence model based on DES formulation to compute a flat plate, a good agreement between experimental and numerical results is presented [23].

Turbulent parameters are defined by specifying the turbulence intensity and hydraulic diameter in this work. Total pressure is set at pump turbine inlet, whereas opening condition is adopted at outlet due to highly disturbed flow field in the draft tube. Different

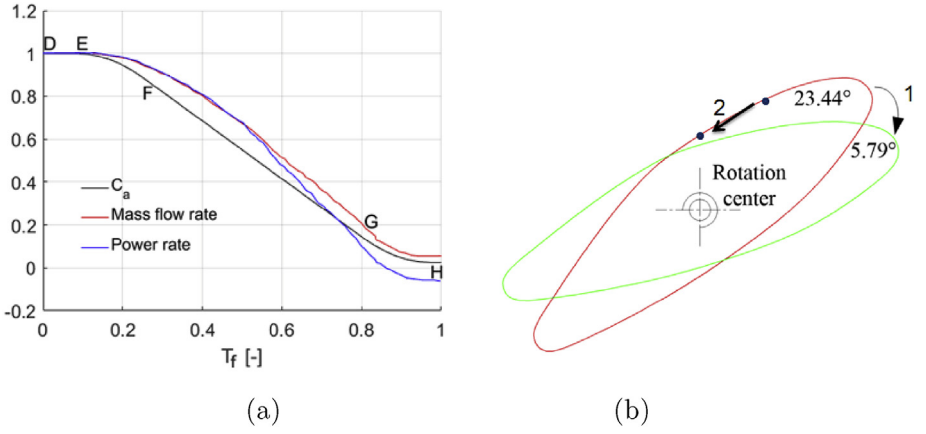

Fig. 5. Guide vane closing law and mesh movement directions.

domains are connected with interfaces(GGI), rotor-stator interfaces are set with FRI in steady simulations and TR/SI in transient simulations. Solid walls are defined as no-slip, scalable wall functions are used in steady simulations while automatic near wall treatment is applied in unsteady simulation. All simulations are done in one multi-core computer with 8 cores, the transient calculating process needs about 20 days to finish.

Monitoring points in flow field are set for acquiring pressure signals as shown in Fig. 6. Pressure fluctuating signals that obtained from numerical simulations will be considered as sound source in this work.

2.3. Mesh and setup in sound field

LMS Virtual Lab Acoustic software is used to study flow induced noise in sound field. For the sake of guaranteeing the accuracy of acoustic calculations, presuming that each wavelength contains 6 acoustic mesh cells at least according to acoustic boundary element method. Similar way in the previous work as shown in Ref. [24] is implemented to analyse flow induced noise. Fig. 7(a) presents shell grid with about 1.05 million elements which unit length equals to 10 mm. The material selects gray cast iron and its density is 7200 kg/m^3, elastic modulus E = 148 GPa, Poisson's ratio is defined as 0.3, damping coefficient ratio is 0.01. The internal sound field medium is water which density equals to $1000kg/m^3$, sound velocity can be taken as $1500m/s$ according to experiences, reference pressure is set as $1 \times 10^{-6}Pa$. The external sound field medium is air which density equals to 1.225 kg/m^3, sound velocity in air is 340 m/s.

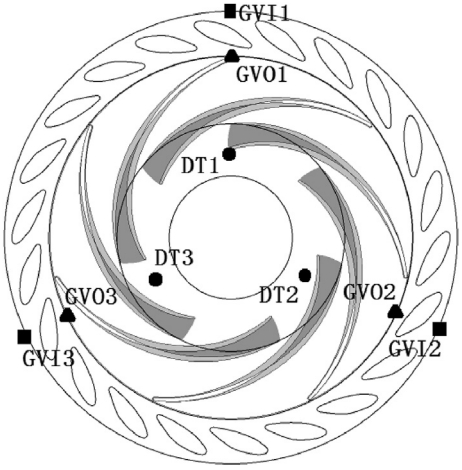

Fig. 6. Locations of some monitoring points in RPT, Guide vane inlet:GVI1,GVI2,GVI3; Guide vane outlet:GVO1,GVO2,GVO3; Draft tube inlet:DT1,DT2,DT3.

Owing to the directionality of sound propagation, the measured noise spectrum depends on locations of monitoring points with respect to directions and distances. For the purpose of analyzing the directivity distribution and radiation level of flow induced noise in pump turbine load rejection process, the runner center is regarded as center of planes. XY plane, YZ plane and XZ plane are built respectively with radius equals to 1.5 m in Fig. 7(b). Each plane is divided into five equal divisions along the radial direction, monitoring points are set at every ten degrees on the demarcation lines(as shown in Fig. 18 and Fig. 19).

3. Results and discussion

This work includes two steps, the first step is numerical calculation for a hydrodynamic analysis in flow field, which provides sound source for the second step. The second step is hydroacoustic analysis in acoustic field comprehensively, the relationship between flow and sound fields is built in this section.

3.1. Analysis of pressure fluctuations in flow field

Fig. 8 shows pressure coefficients acquired from monitoring points at vane inlet and outlet(Fig. 6) during the period of pump turbine load rejection. The pressure change assumes similar trends for the points at the same circumferentially symmetrical positions as shown in Fig. 8(a). The guide vane inlet pressure exhibits a gradual upward tendency, which fluctuating amplitudes keeps decreasing due to the degree of reaction reduction(degree of reaction = the improvement of static pressure energy/theoretical power).

The pressure at vane outlet presents a steady downward trend in Fig. 8(b), and the range of pressure fluctuating amplitudes keeps narrowing until $T_f = 0.67$. Above amplitudes experience expansions in the following time, the main reason is the appearance of detached eddy in vane domain and return channels caused by small flow. This moment is aligned with the time that cavity zone appearance in the draft tube(Fig. 10).

Comparing the pressure PSD trends of points in the

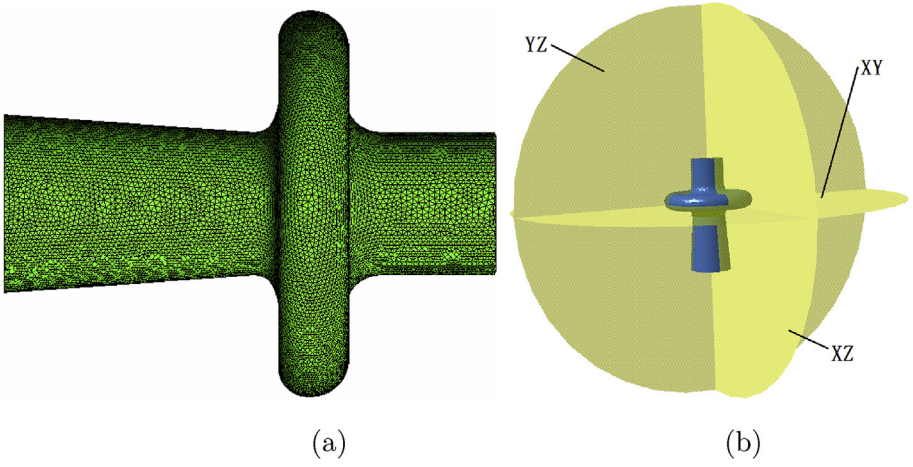

Fig. 7. Mesh of shell and monitoring planes in acoustic field: (a) Acoustic field mesh of RPT, (b) XY, XZ, YZ planes in the acoustic field.

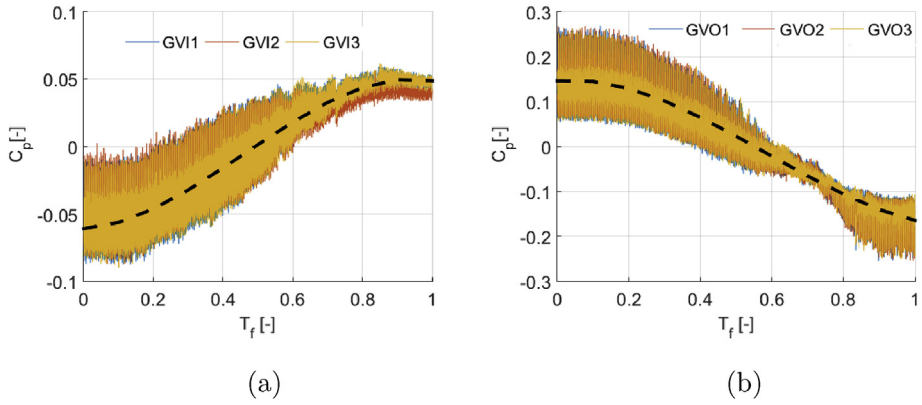

Fig. 8. Pressure coefficients of monitoring points versus the relative time at vane inlet and outlet: (a) Guide vane inlet GVI1, GVI2 and GVI3, (b) Guide vane outlet GVIO, GVO2 and GVO3.

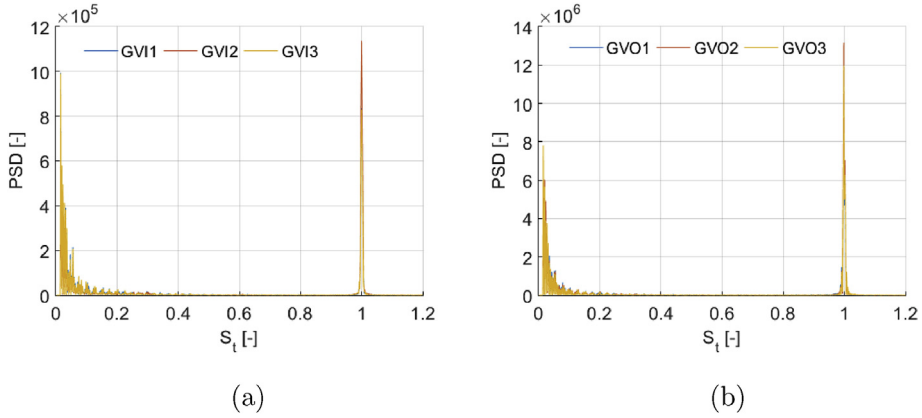

Fig. 9. Normalized Pressure PSD of monitoring points versus Strauhal number at vane inlet and outlet: (a) Guide vane inlet GVI1, GVI2 and GVI3, (b) Guide vane outlet GVO1, GVO2 and GVO3.

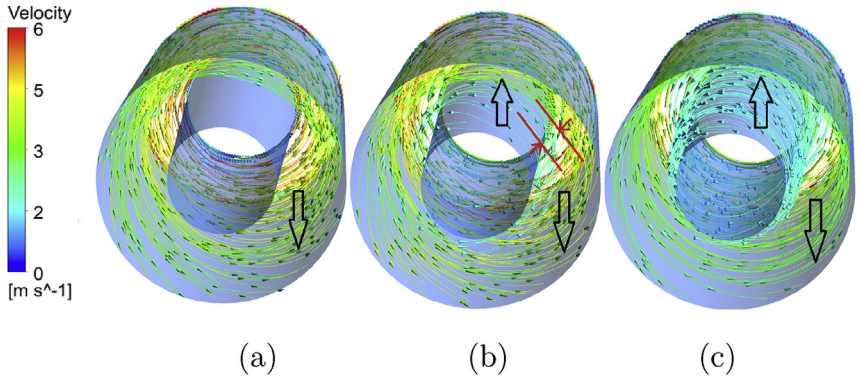

Fig. 10. Streamlines and flow velocity in the draft tube at special moments: (a) A cavity around hub appears at $T_f = 0.64$, (b) Reflux around hub appears with opposite outflow rotating direction at $T_f = 0.67$, (c) A cavity column between different flows with opposite rotating directions at $T_f = 1$.

circumferential direction of guide vane inlet and outlet shows similar characteristics as shown in Fig. 9. The autospectral of pressure signals are dominated by a peak at $St_{RS,rot} = 0.051$. It is worth mentioning that the blade passage frequency(BPF) is much more pronounced in pressure autospectra($St_{BPF,st} = 1$), due to the runner blades rotation affect the pressure pulsations significantly.

PSD amplitudes of guide vane outlet in Fig. 9(b) are higher than the portion of guide vane inlet in Fig. 9(a), which is around 10 times. It illustrates that the influence of rotor-rotor interaction on internal flow field is stronger than the influence of rotor-stator interaction.

The evolution of pressure in the draft tube is presented for three different instants in time(Fig. 11(a)), which corresponds to the three stages of flow field change in Fig. 10. Initially, The rotating outflow fills the whole pipe, which direction coincides with runner rotating direction, and the flow adjoins the pipe walls without separation. In Fig. 10(a), from beginning to $T_f = 0.64$, the flow in the draft tube forwards to shroud and forms a cavity around hub, the main reason is the flow rate reduction. Reflux around hub appears with the

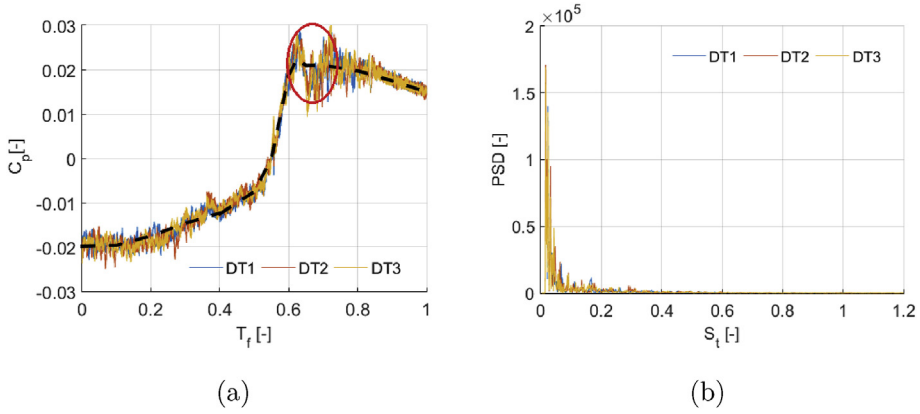

Fig. 11. (a) Pressure coefficients versus relative time and (b) normalized pressure PSD amplitudes versus Strauhal number of monitoring points DT1, DT2 and DT3.

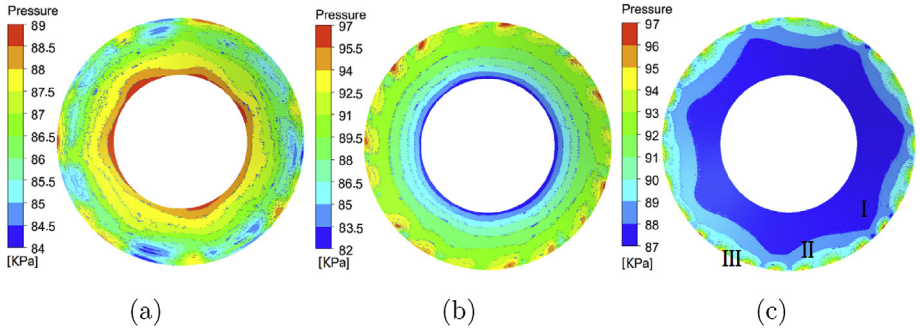

Fig. 12. Inlet gauge pressure distributions registered at draft tube inlet: (a) $T_f = 0.64$, (b) $T_f = 0.67$, (c) $T_f = 1$.

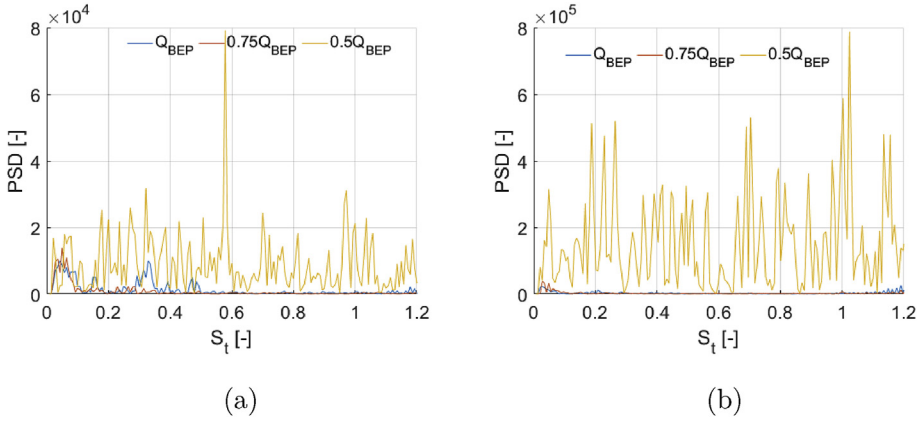

Fig. 13. Normalized PSD of pressure signals with special flows at Q_{BEP}, $0.75Q_{BEP}$ and $0.5Q_{BEP}$: (a) Guide vane inlet GVI1, (b) Guide vane outlet GVO1.

opposite rotating direction at $T_f = 0.67$ as shown in the Fig. 10(b), due to flow reduction and runner outflow circulation influence. Red lines in Fig. 10(b) indicates a cavity column between outflow and backflow, and the pressure amplitudes in red elliptical area in Fig. 11(b) changes dramatically is correlated to this. Fig. 10(c) presents this cavity column becomes smaller, due to reflux around hub is more severe at $T_f = 1$.

Pressure signals at draft tube monitoring points are given in Fig. 11. From Fig. 11(b) a peak at $St_{RS,rot} = 0.051$ dominates the resulting power spectrum. The BPF($St_{BPF,st} = 1$) is detected weakly in the spectrum on account of the development of unsteady flow field.

Fig. 12 is pressure cloud maps of draft tube inlet at corresponding moments in Fig. 10. Three different pressure lever regions are shown clearly in Fig. 12(c). Particularly, region i represents flow column adjoins wall with similar runner rotating direction. Region ii is the cavity column and region iii is the flow column around wall with opposite rotating direction. The seven lower pressure areas at the wall of the draft tube cone are caused by runner rotation, and they correlate to the runner passages and the development of their wake(Fig. 12(c)).

Normalized power spectral density of pressure characteristics obtained at stable guide vane conditions are given in Figs. 13 and 14, for the sake of analyzing flow field under intermittent guide vane

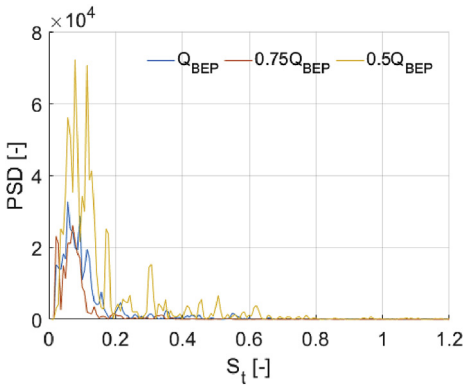

Fig. 14. Normalized PSD of pressure signals with special flows at Q_{BEP}, $0.75Q_{BEP}$ and $0.5Q_{BEP}$ acquired from monitoring point DT1.

closure conditions. The most notable feature is the difference of amplitudes, the pressure evolutions and amplitudes of each monitoring points are similar at Q_{BEP} and $0.75Q_{BEP}$, under $0.5Q_{BEP}$ conditions. The pressure signal amplitudes are greater than the relative values of larger flows in each figure of Figs. 13 and 14. Various frequency peaks are captured in different positions, corresponding peaks at vane outlet is 10 times of the relative acquisitions from vane inlet and draft tube. It is similar to results of continuous vane closure as shown in Figs. 9 and 11. The main reason of this phenomenon in fixed vane conditions is rotor-stator interaction. In addition to the above mentioned, PSD at homologous locations(vane inlet and outlet, runner outlet) of transient process is with one more magnitude than that of fixed vane conditions.

Comparing pressure characteristics of continuous vane closure process and intermittent vane closing conditions, the results show frequency peaks are only captured under $0.5Q_{BEP}$ conditions markedly of the latter. It is interesting to notice that $St = 0.58$ is much more pronounced in the auto-spectra of the distributor signals at vane inlet, which associates with runner rotating frequency. Pressure pulsations caused by runner blades rotation are strongly perceived at vane outlet, BPF is detected at vane outlet exclusively. Significant peaks appear around $St = 0.093$ (65.1% of runner rotation frequency) which is related to runner rotation frequency in the rotating frame.

3.2. Analysis of flow induced noise in sound field

The trends of hydraulic mechanical flow induced noise directivity distribution in all directions are basically the same, which does not vary with flow change [25]. Consequently, the plane XY is chosen to study noise distribution in the external acoustic field as shown in following figures. The noise directivity distribution and radiation level at the first, second and third order blade passage frequencies are the emphasis of this part analysis.

Acoustic pressure level distribution under special flow conditions are presented in Figs. 15–17. They illustrate that the blade surface dipole sound source corresponding to these sound cloud maps with distinct ″∞″ embodiment. The distribution of sound pressure show significant symmetry on the XY plane at each order BPF, which in turn proves that the blade noise radiation has obvious dipole characteristics.

The sound pressure diffusion shape is associated with pump turbine structure as shown in Figs. 15–17. Sound pressure amplitudes are symmetrically attenuated in the axial and perpendicular

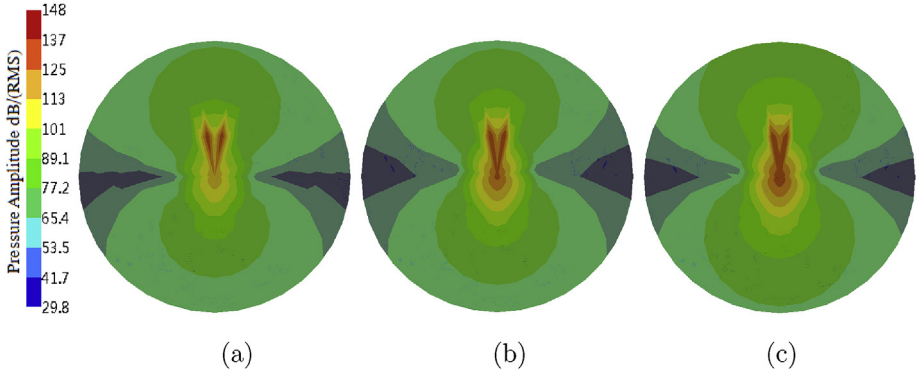

Fig. 15. Acoustic pressure level under the condition of flow rate equals to Q_{BEP}:(a) First order BPF, (b) Second order BPF, (c) Third order BPF.

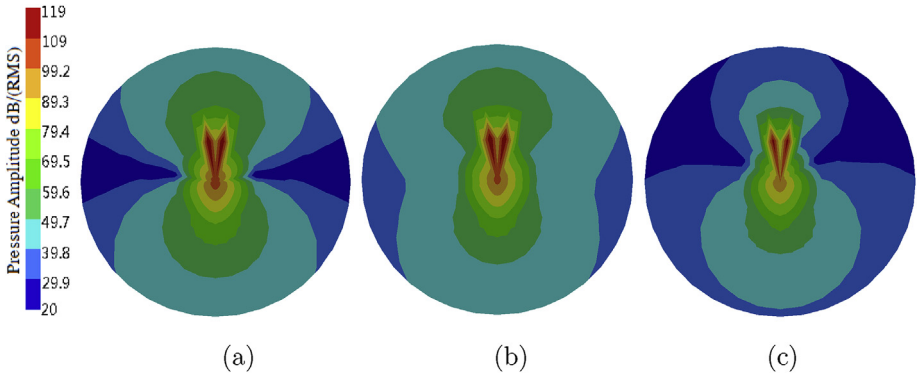

Fig. 16. Acoustic pressure level under the condition of flow rate equals to $0.5Q_{BEP}$: (a) First order BPF, (b) Second order BPF, (c) Third order BPF.

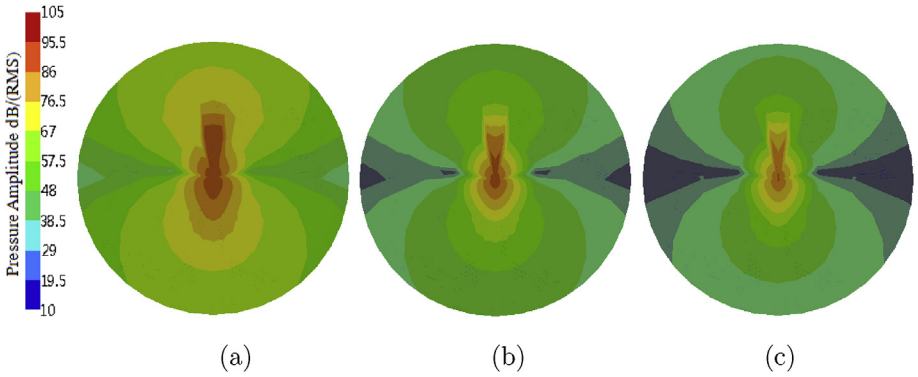

Fig. 17. Acoustic pressure level under the condition of flow rate equals to $0.1Q_{BEP}$: (a) First order BPF, (b) Second order BPF, (c) Third order BPF.

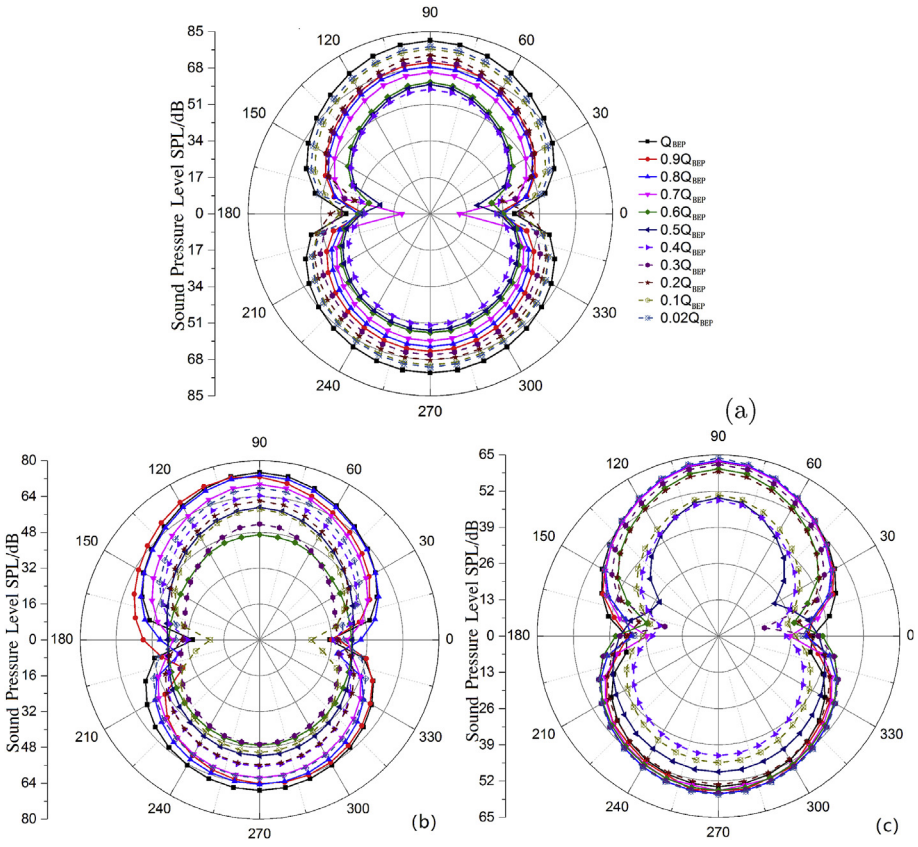

Fig. 18. Sound pressure level distribution for analyzing acoustic directivity of pump turbine in the continuous load rejection process: (a) First order BPF, (b) Second order BPF, (c) Third order BPF.

to the axial flow directions. As for the sound pressure amplitudes acquired from the location of pump turbine model in these cloud maps, they are larger than other regions and they decrease with increasing distance from model. Sword-toothed area with red color explains the highest sound pressure value in the draft tube, which correlates to the intricate flow field(Fig. 10). Combining analysis of these cloud maps (Figs. 15–17), the flow induced noise pressure range maintains a downward tendency as flow dwindle. The sound pressure range reduces by approximately 20% under $0.1Q_{BEP}$ condition compared to the circumstance under Q_{BEP} condition.

Fig. 18 is a detailed stepwise illustration of acoustic radiation level of pump turbine in continuous load rejection process. With reference to cloud Figs. 15–17, sound pressure radiation level at the first BPF is higher than corresponding values at other two BPF orders. The main reason is one of the specified natural frequency of pump turbine shell approximates to the first order BPF, which causes higher acoustic radiation level. Simultaneously, from another perspective view of the obvious phenomenon, it demonstrates that the main frequency of flow induced noise is determined by the main frequency of pressure pulsation and natural frequency of the shell concurrently. It should be considered in model design, for the sake of avoiding BPF is similar to natural frequency of shell.

As for sound pressure signals collected under different flow conditions in the analyses with distinctive BPF orders (Fig. 18), the minimum sound pressure values are located at 0° and 180°. However, the maximum value is close to 90° position that is near to

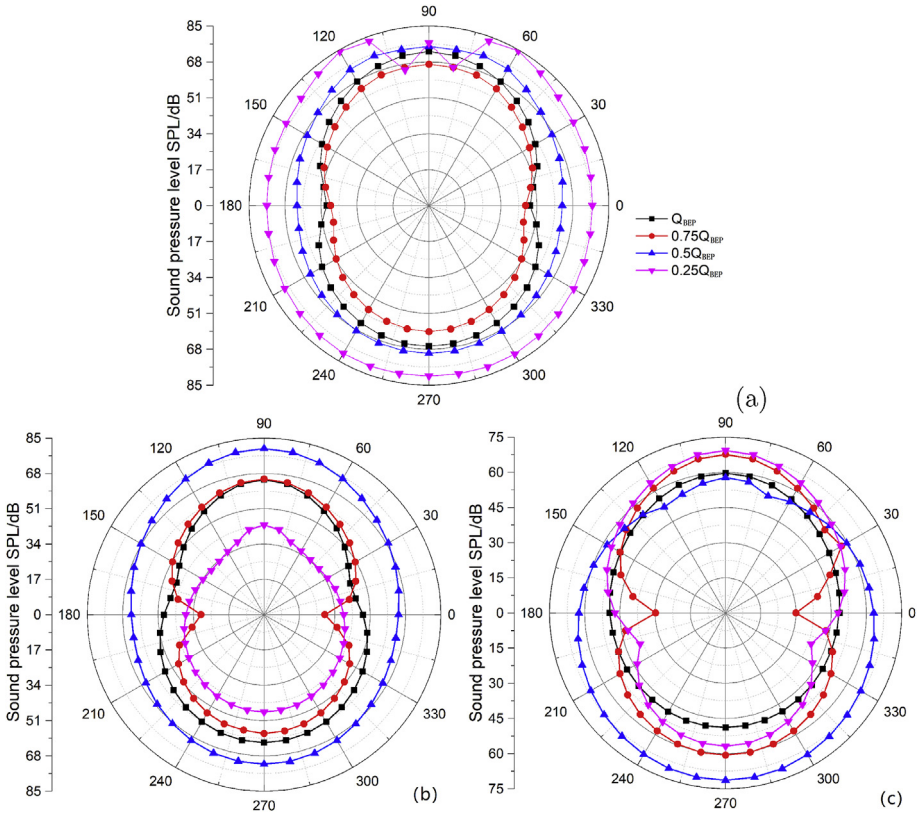

Fig. 19. Acoustic directivity of pump turbine under special flows with fixed vane openings: (a) First order BPF; (b) Second order BPF; (c) Third order BPF.

draft tube. The causes of this phenomenon is considered to be the following: the flow in the draft tube is affected by the runner rotation which has a certain circumferential velocity to generate swirl; the water in the draft tube is not great enough to supplement the cavity due to flow reduction, which aggravates vortex generation in this domain.

In Fig. 18(a), the first order BEP sound pressure level declines gradually from the beginning to 50% guide vane closure, whereas it keeps an upward trend in the following guide vane closing process.

In case of second order BPF data about acoustic pressure radiation development, Fig. 18(b) shows the results corresponding to flow field variation in draft tube(Fig. 10). The sound pressure level goes down with flow decrease until $0.6Q_{BEP}$, and the value of sound pressure level at Q_{BEP} is 1.5 times of that at $0.6Q_{BEP}$. In the following process of flow reduction from $0.6Q_{BEP}$ to $0.4Q_{BEP}$, acoustic level of second order BPF becomes larger due to formation of swirling flow in the draft tube cavity region. As the space between outflow zone and recirculation zone narrow in draft tube(Fig. 10), the sound pressure level continues to decrease until water flow is not enough to fill this space. From $0.3Q_{BEP}$ to $0.02Q_{BEP}$, the sound pressure level shows an increasing trend.

Acoustic pressure level of the third order BPF basically unchanged during the period from beginning to $0.7Q_{BEP}$ in Fig. 18(c). In the process of further flow reduction until $0.5Q_{BEP}$, the results show a significant drop. During the last 50% guide vane closing period, acoustic pressure level presents disordered developing tendency. In conclusion, flow change has a considerable influence on flow induced noise radiation level, and acoustic pressure level change is related to pump turbine internal flow field variation during the period of continuous load rejection.

Flow induced noise distribution under intermittent vane closure conditions with special flows(Q_{BEP}, $0.75Q_{BEP}$, $0.5Q_{BEP}$) are given in Fig. 19. The sound pressure levels at first order BPF are shown as elliptical shapes, this illustrates that acoustic pressure radiation is similar in axisymmetrical directions. Dipole characteristics are only pronounced with the second and third orders at $0.75Q_{BEP}$ as shown in Fig. 19(b)and(c). The sound pressure levels are smaller than the corresponding values that monitored in load rejection process, and this point interprets extreme instability of transient fluid from another point of view.

In comparison with larger flow conditions, acoustic level acquired from $0.5Q_{BEP}$ is greater due to the intensified instability of internal flow field. The ellipse is close to circles gradually at higher orders under the condition with $0.5Q_{BEP}$, which explains the external noise radiation intensities in various directions are almost equivalent.

Curves of $0.25Q_{BEP}$ are exclusively used to reflect distinctive between fixed vane calculation and continuous vane closure. The results provides a further illustration about a fact that load rejection simulation can not be replaced by fixed vane calculations. However, the evolution of sound pressure level are similar in these two kinds of vane closing simulations.

4. Conclusions

In this work, a validated model is used to simulate continuous and intermittent guide vane closing processes based on DES turbulence model. Both flow field and sound field are studied to investigate pump turbine operating instability.

Rotor-rotor interaction influence on flow field is stronger than that of rotor-stator interaction during the continuous load rejection period. The pressure fluctuating amplitudes at vane outlet is more than twice compared to the relative value acquired from vane inlet. The vane outlet pressure PSD magnitudes are 10 times of the

relative values obtained from the inlet. The flow induced noise radiation is consistent with fluid characteristics during the period of pump turbine load rejection. Its radiation level is determined by the pressure fluctuating frequency and shell natural frequency. In addition, the shape of sound distribution likes "∞" and sound level in different directions and faces are symmetrical.

PSD at homologous locations of transient load rejection is with one more magnitude than that of fixed vane conditions. Runner rotating frequency is only highlighted with vane inlet pressure information in the part of intermittent vane closure analysis. The blade frequency is more pronounced with vane outlet under $0.5Q_{BEP}$ condition. On the aspect of flow induced noise, significantly the results of fixed vane conditions are different from data acquired from continuous vane closing process based on same flows. However, both fixed vane calculations and continuous vane closure obtained similar flow induced noise developing tendency. In conclusion, acoustic pressure radiation reflects flow field development from another point of view, which can be improved by controlling pressure pulsations of fluid. This work provides a reference for the study of pump turbine stability problems from the combination of flow field and acoustic aspect.

Acknowledgements

This work was supported by the research start-up fundation of Northwest A& F University(Z109021813).

Nomenclature

α	Blade angle°
B_{RI}	Width of runner inletmm
B_{GVO}	Width of guide vane outletmm
B_{RTO}	Width of return channel outletmm
$BPF = \frac{N_{RB}n}{60}$	Blade passage frequency Hz
Ca	Relative opening of guide vane
$C_p = \frac{p-\bar{p}}{\bar{p}}$	Pressure coefficient
D_{GVO}	Diameter of guide vane outletmm
D_{RI}	Diameter of runner inletmm
D_{RTO}	Diameter of return channel outletmm
H	Headm
n_R	Number of runner blades
n_{GV}	Number of guide vanes
n_{RT}	Number of return channels
P	Pressure Pa
Q	Mass flow kg/s
$St = \frac{f}{BPF}$	Strouhal number
t	Times
$T_f = \frac{t}{t_{max}}$	Time factor
V	Velocity m/s
x	Distance alongside pipe m
α	Blade angle°

Abbreviations

BEP	Best efficient point
BPF	Blade passage frequency
CFD	Computational Fluid Dynamics
DES	Detached Eddy Simulation
DF	Draft tube
FRI	Frozen Rotor Interface
GGI	General Grid Interface
GVI	Guide vane inlet
GVO	Guide vane outlet
SST	*ShearStressTransport*
LES	Large Eddy Simulation
PSD	Power spectra density
RANS	Reynolds Average Navier-Stokes
RPT	Reversible pump turbine
TR/SI	Transient Rotor/Stator Interface

References

[1] W. Yang, P. Norrlund, L. Saarinen, A. Witt, B. Smith, J. Yang, U. Lundin, Burden on hydropower units for short-term balancing of renewable power systems, Nat. Commun. 9 (2633) (2018) 1–12, https://doi.org/10.1038/s41467-018-05060-4.

[2] A. Ghasemi, M. Enayatzare, Optimal energy management of a renewable-based isolated microgrid with pumped-storage unit and demand response, Renew. Energy 123 (2018) 460–474, https://doi.org/10.1016/j.renene.2018.02.072.

[3] C.L. Chen, H.C. Chen, J.Y. Lee, Application of a generic superstructure-based formulation to the design of wind-pumped-storage hybrid systems on remote islands, Energy Convers. Manag. 111 (2016) 339–351, https://doi.org/10.1016/j.enconman.2015.12.057.

[4] J.H. Kim, B.M. Cho, S. Kim, J.W. Kim, J.W. Suh, Y.S. Choi, T. Kanemoto, J.H. Kim, Design technique to improve the energy efficiency of a counter-rotating type pump-turbine, Renew. Energy 101 (2017) 647–659, https://doi.org/10.1016/j.renene.2016.09.026.

[5] G. Olimstad, T. Nielsen, B. Brresen, Stability limits of reversible-pump turbines in turbine mode of operation and measurements of unstable characteristics, J. Fluid Eng. 134 (11) (2012) 872–882, https://doi.org/10.1115/1.4007589.

[6] M. Xiuli, P. Giorgio, Z. Yuan, Francis-type reversible turbine field investigation during fast closure of wicket gates, J. Fluid Eng. 140 (6) (2018), 061103, https://doi.org/10.1115/1.4039089.

[7] S. Holler, H. Benigni, H. Jaberg, Investigation of the 4-quadrant behaviour of a mixed flow diffuser pump with cfd-methods and test rig evaluation, in: IOP Conference Series: Earth and Environmental Science, 2016, 032018, https://doi.org/10.1088/1755-1315/49/3/032018.

[8] E. Walseth, T. Nielsen, B. Svingen, Measuring the dynamic characteristics of a low specific speed pumpturbine model, Energies 9 (3) (2016) 199, https://doi.org/10.3390/en9030199.

[9] T. Guo, L. Zhang, W. Wang, Z. Luo, Rotating turbulent flow simulation with les and vreman subgrid-scale models in complex geometries, Adv. Mech. Eng. 6 (4) (2014), https://doi.org/10.1155/2014/570189, 570189–570189.

[10] K.H. Liu, Y.N. Zhang, J.W. Li, H.Z. Xian, Quantitative analysis of backflow of reversible pump-turbine in generating mode, in: IOP Conference Series: Materials Science and Engineering vol. 129, 2016, 012027, https://doi.org/10.1088/1757-899X/129/1/012027.

[11] A. Rezghi, A. Riasi, Sensitivity analysis of transient flow of two parallel pump-turbines operating at runaway, Renew. Energy 86 (2016) 611–622, https://doi.org/10.1016/j.renene.2015.08.059.

[12] H. Zhang, D. Chen, B. Xu, F. Wang, Nonlinear modeling and dynamic analysis of hydro-turbine governing system in the process of load rejection transient, Energy Convers. Manag. 90 (2015) 128–137, https://doi.org/10.1016/j.enconman.2014.11.020.

[13] Y. Heng, S. Yuan, F. Hong, J. Yuan, Q. Si, B. Hu, A hybrid method for flow-induced noise in centrifugal pumps based on les and fem, in: ASME 2013 Fluids Engineering Division Summer Meeting, 2013, https://doi.org/10.1115/FEDSM2013-16594. V01BT10A034–V01BT10A034.

[14] M.A. Langthjem, N. Olhoff, A numerical study of flow-induced noise in a two-dimensional centrifugal pump. part i. hydrodynamics, J. Fluid Struct. 19 (3) (2004) 349–368, https://doi.org/10.1016/j.jfluidstructs.2004.01.003.

[15] R. Dong, S. Chu, J. Katz, Effect of modification to tongue and impeller geometry on unsteady flow, pressure fluctuations, and noise in a centrifugal pump, J. Turbomach. 119 (3) (1997), https://doi.org/10.1115/1.2841152. V001T01A005.

[16] Y. Yamade, H. Wang, Y. Guo, M. Miyazawa, Numerical prediction of sound generated from flows with a low mach number, Comput. Fluids 36 (1) (2007) 53–68, https://doi.org/10.1016/j.compfluid.2005.07.006.

[17] J. Parrondo, J. Prez, R. Barrio, J. Gonzlez, A simple acoustic model to characterize the internal low frequency sound field in centrifugal pumps, Appl. Acoust. 72 (1) (2011) 59–64, https://doi.org/10.1016/j.apacoust.2010.08.005.

[18] L. Houlin, D. Hanwei, D. Jian, T. Gaoming, W. Yong, H. Haoqin, Numerical and experimental studies of hydraulic noise induced by surface dipole sources in a centrifugal pump, J. Hydrodyn. Ser. B 28 (1) (2016) 43–51, https://doi.org/10.1016/S1001-6058(16)60606-6.

[19] Y. Jun, Y. Shouqi, S. Qiaorui, Numerical and experimental study on flow-induced noise at blade-passing frequency in centrifugal pumps, Chin. J. Mech. Eng. 27 (3) (2014) 606–614, https://doi.org/10.3901/CJME.2014.03.606.

[20] A.V. Minakov, A.V. Sentyabov, D.V. Platonov, A.A. Dekterev, A.A. Gavrilov, Numerical modeling of flow in the francis-99 turbine with Reynolds stress model and detached eddy simulation method, J. Phys. Conf. 579 (2015), 012004, https://doi.org/10.1088/1742-6596/579/1/012004.

[21] H.Y. Xu, C.L. Qiao, H.Q. Yang, Z.Y. Ye, Delayed detached eddy simulation of the wind turbine airfoil s809 for angles of attack up to 90 degrees, Energy 118 (2016) 1090–1109, https://doi.org/10.1016/j.energy.2016.10.131.

[22] E. Guilmineau, G.B. Deng, J. Wackers, Numerical simulation with a des approach for automotive flows, J. Fluid Struct. 27 (56) (2010) 807–816, https://doi.org/10.1016/j.jfluidstructs.2011.03.010.
[23] H. Xu, T. Wray, R.K. Agarwal, A new des model based on wray-agarwal turbulence model for simulation of wall-bounded flows, in: Aiaa Aerospace Sciences Meeting, vol. 0, 2016, pp. 1–8, https://doi.org/10.2514/6.2016-0612.
[24] Y. Zheng, Y. Chen, X. Mao, H. Wang, W. Shi, K. Kan, Y. Zhang, Pressure pulsation characteristics and its impact on flow-induced noise in mixed-flow pump, Trans. Chin. Soc. Agric. Eng. 31 (23) (2015) 67–73, https://doi.org/10.11975/j.issn.1002-6819.2015.23.009.
[25] E. Chen, Z. Ma, G. Zhao, G. Li, A. Yang, G. Nan, Numerical investigation on vibration and noise induced by unsteady flow in an axial-flow pump, J. Mech. Sci. Technol. 30 (12) (2016) 5397–5404, https://doi.org/10.1007/s12206-016-1107-4.